VISUAL INTERPRETABILITY ALONE HELPS ADVERSARIAL ROBUSTNESS

Anonymous authors
Paper under double-blind review

ABSTRACT

Recent works have empirically shown that there exist adversarial examples that can be hidden from neural network interpretability, and interpretability is itself susceptible to adversarial attacks. In this paper, we theoretically show that with the correct measurement of interpretation, it is actually *difficult* to hide adversarial examples, as confirmed by experiments on MNIST, CIFAR-10 and Restricted ImageNet. Spurred by that, we develop a novel defensive scheme built only on robust interpretation (without resorting to adversarial loss minimization). We show that our defense achieves similar classification robustness to state-of-the-art robust training methods while attaining higher interpretation robustness under various settings of adversarial attacks.

1 INTRODUCTION

It has become widely known that convolutional neural networks (CNNs) are vulnerable to *adversarial examples*, namely, perturbed inputs with intention to mislead networks' prediction (Szegedy et al., 2014; Goodfellow et al., 2015; Papernot et al., 2016a; Carlini & Wagner, 2017; Chen et al., 2018; Su et al., 2018). The vulnerability of CNNs has spurred extensive research on adversarial attack and defense. To design adversarial attacks, most work has focused on creating either imperceptible input perturbations (Goodfellow et al., 2015; Papernot et al., 2016a; Carlini & Wagner, 2017; Chen et al., 2018) or adversarial patches robust to the physical environment (Eykholt et al., 2018; Brown et al., 2017; Athalye et al., 2017). Many defense methods have also been developed to prevent CNNs from misclassification when facing adversarial attacks. Examples include defensive distillation (Papernot et al., 2016b), training with adversarial examples (Goodfellow et al., 2015), input gradient or curvature regularization (Ross & Doshi-Velez, 2018; Moosavi-Dezfooli et al., 2019), adversarial training via robust optimization (Madry et al., 2018), and TRADES to trade adversarial robustness off against accuracy (Zhang et al., 2019). Besides studying adversarial effects on network prediction decisions, this work explores the connection between adversarial robustness and network interpretability, and provides novel insights on when and how interpretability helps the robustness.

Having a prediction might not be enough for many real-world machine learning applications. It is also crucial to demystify why CNNs make certain decisions. Thus, the problem of network interpretation arises. Various methods have been proposed to understand the mechanism of decision making by CNNs. One category of methods justify a prediction decision by assigning importance values to reflect the influence of individual pixels or image sub-regions on the final classification. Examples include pixel-space sensitivity map methods (Simonyan et al., 2013; Zeiler & Fergus, 2014; Springenberg et al., 2014; Smilkov et al., 2017; Sundararajan et al., 2017) and class-discriminative localization methods (Zhou et al., 2016; Selvaraju et al., 2017; Chattopadhay et al., 2018; Petsiuk et al., 2018), where the former evaluates the sensitivity of a network classification decision to pixel variations at the input, and the latter localizes which parts of an input image were looked at by the network for making a classification decision. Sensitivity map methods include vanilla gradient (Simonyan et al., 2013), deconvolution (Zeiler & Fergus, 2014), guided backpropagation (Springenberg et al., 2014), SmoothGrad (Smilkov et al., 2017), integrated gradient (IG) (Sundararajan et al., 2017) to name a few. They highlight fine-grained details in the image but are not class-discriminative for visual explanation. By contrast, localization approaches like class activation map (CAM) (Zhou et al., 2016), GradCAM (Selvaraju et al., 2017), GradCAM++ (Chattopadhay et al., 2018) and RISE (Petsiuk et al., 2018) are highly class-discriminative, namely, localizing image sub-regions reasoned for a prediction class. We refer readers to Sec. 2 for some representative interpretation methods.

Besides interpreting CNNs via feature importance maps, some methods zoom into the internal response of neural networks. Examples include network dissection (Bau et al., 2017), which evaluates the alignment between individual hidden units and semantic concepts, and learning perceptually-aligned representations from robust training (Engstrom et al., 2019).

Very recently, some works (Xu et al., 2019b;a; Zhang et al., 2018; Subramanya et al., 2018; Ghorbani et al., 2019; Dombrowski et al., 2019; Chen et al., 2019) are beginning to study adversarial robustness by exploring the spectrum between classification accuracy and network interpretability. It was shown in (Xu et al., 2019b;a) that an imperceptible adversarial perturbation to fool classifiers can lead to a significant change in a class-specific network interpretability map, e.g., CAM. Thus, it was argued that such an *interpretability discrepancy* can be used as a helpful metric to differentiate adversarial examples from benign inputs. However, the work (Zhang et al., 2018; Subramanya et al., 2018) showed that under certain conditions, generating an attack (which we call *interpretability sneaking attack, ISA*) that fools the classifier as well as its coupled interpreter (in terms of keeping interpretability map highly similar to that of benign input) is not significantly more difficult than generating adversarial inputs deceiving the classifier only. The existing work had *no agreement* on whether or not it is really easy for adversarial examples to fool the interpreter. Besides investigating robustness in classification through the lens of interpretability, the work (Ghorbani et al., 2019; Dombrowski et al., 2019) studied the robustness in interpretability and showed that network interpretation maps can significantly be manipulated via imperceptible input perturbations but keeping classifier's decision *intact*. We call this type of threat model *attack against interpretability (AAI)*. The most relevant work to ours is (Chen et al., 2019), which robustified network interpretation with the aid of integrated gradient (IG), an axiomatic attribution map. It proposed a robust attribution training, which was shown as a principled generalization of previous formulations of robust classification and an effective defense against AAI. Different from the previous work, our paper contains the following contributions.

1. We show that enforcing stealthiness of adversarial examples from network interpretation could be challenging. Its difficulty relies on how one measures the interpretability discrepancy caused by input perturbations.
2. We propose an ℓ_1 norm based 2-class interpretability discrepancy measure and theoretically show that constraining it helps adversarial robustness.
3. We develop an interpretability-aware robust training method and empirically show that interpretability alone can be used to defend adversarial attacks for both misclassifcation and misinterpretation. Compared to the IG-based robust attribution training (Chen et al., 2019), our approach is simpler in implementation, and provides better robustness even as facing a strong adversary.

2 Preliminaries and Motivation: Interpretability of CNNs for Justifying A Classification Decision

To explain what and why CNNs predict, we consider two types of network interpretation methods: a) *class activation map (CAM)* and b) *pixel sensitivity map (PSM)*. The former localizes a class-discriminative image region that explains which parts of an input image are focused by the CNN for assigning a class label (Zhou et al., 2016; Selvaraju et al., 2017; Chattopadhay et al., 2018). The latter evaluates the importance of individual input pixels by finding the sensitivity of classification decision to a tiny change at these pixels (Simonyan et al., 2013; Springenberg et al., 2014; Smilkov et al., 2017; Sundararajan et al., 2017; Yeh et al., 2019).

Let $f(\mathbf{x}) \in \mathbb{R}^C$ denote a CNN-based predictor that maps an input $\mathbf{x} \in \mathbb{R}^d$ to a probability vector of C classes. Here $f_c(\mathbf{x})$, the cth element of $f(\mathbf{x})$, denotes the classification score (given by logit before the softmax) for class c. Let $L(\mathbf{x}, c)$ denote an interpreter (CAM or PSM) that reflects where in $\mathbf{x}$ contributes to the classifier's decision on c.

CAM-type methods. CAM (Zhou et al., 2016) produces a class-discriminative localization map for CNNs, which performs global averaging pooling over convolutional feature maps prior to the softmax. Let the penultimate layer output K feature maps, each of which is denoted by a vector representation $\mathbf{A}_k \in \mathbb{R}^u$ for channel $k \in [K]$. Here $[K]$ represents the integer set $\{1, 2, \ldots, K\}$.

The ith entry of CAM $L_{\mathrm{CAM}}(\mathbf{x}, c)$ is given by

$$[L_{\mathrm{CAM}}(\mathbf{x}, c)]_i = \frac{1}{u} \sum_{k \in [K]} w_k^c A_{k,i},\ i \in [u], \tag{1}$$

where w_k^c is the linear classification weight that associates the channel k with the class c, and $A_{k,i}$ denotes the ith element of $\mathbf{A}_k$. The rationale behind (1) is that the classification score $f_c(\mathbf{x})$ can be written as the average of CAM values (Zhou et al., 2016), $f_c(\mathbf{x}) = \sum_{i=1}^u [L_{\mathrm{CAM}}(\mathbf{x}, c)]_i$. For visual explanation, $L_{\mathrm{CAM}}(\mathbf{x}, c)$ is often up-sampled to the input dimension d using bi-linear interpolation.

GradCAM (Selvaraju et al., 2017) generalizes CAM for CNNs without the architecture 'global average pooling → softmax layer' over the final convolutional maps. Specifically, the weight w_k^c in (1) is given by the gradient of the classification score $f_c(\mathbf{x})$ with respect to (w.r.t.) the feature map $\mathbf{A}_k$, $w_k^c = \frac{1}{u} \sum_{i=1}^u \frac{\partial f_c(\mathbf{x})}{\partial A_{k,i}}$. GradCAM++ (Chattopadhay et al., 2018), a generalized formulation of GradCAM, utilizes a more involved weighted average of the (positive) pixel-wise gradients but provides a better localization map if an image contains multiple occurrences of the same class. In this work, we focus on CAM since it is computationally light and our models used in experiments follow the architecture 'global average pooling → softmax layer'.

PSM-type methods. PSM uses calculations with gradients to assign importance scores to individual pixels toward explaining the classification decision about an input. Examples of commonly-used approaches include vanilla gradient (Simonyan et al., 2013), guided backpropogation (Springenberg et al., 2014), SmoothGrad (Smilkov et al., 2017), and integrated gradient (IG) (Sundararajan et al., 2017). In particular, IG satisfies the *completeness* attribution axiom that PSM ought to obey. Specifically, it averages gradient saliency maps for interpolations between an input $\mathbf{x}$ and a baseline image $\mathbf{a}$:

$$[L_{\mathrm{IG}}(\mathbf{x}, c)]_i = (x_i - a_i) \int_{\alpha=0}^{1} \frac{\partial f_c(\mathbf{a} + \alpha(\mathbf{x} - \mathbf{a}))}{\partial x_i} d\alpha \approx (x_i - a_i) \sum_{i=1}^{m} \frac{\partial f_c(\mathbf{a} + \frac{i}{m}(\mathbf{x} - \mathbf{a}))}{\partial x_i} \frac{1}{m},\ i \in [d], \tag{2}$$

where m is the number of steps in the Riemman approximation of the integral. The *completeness* axiom (Sundararajan et al., 2017, Proposition 1) states that $\sum_{i=1}^d [L_{\mathrm{IG}}(\mathbf{x}, c)]_i = f_c(\mathbf{x}) - f_c(\mathbf{a})$, where the baseline image $\mathbf{a}$ is often chosen such that $f_c(\mathbf{a}) \approx 0$, e.g., the black image. Note that CAM also satisfies the *completeness* axiom. PSM is able to highlight fine-grained details in the image, but is computationally intensive and not very class-discriminative compared to CAM (Selvaraju et al., 2017).

Interpretability discrepancy caused by adversarial perturbation. Let $\mathbf{x}' = \mathbf{x} + \boldsymbol{\delta}$ represent an *adversarial example* w.r.t. $\mathbf{x}$, where $\boldsymbol{\delta}$ denotes an *adversarial perturbation*. By replacing the input image $\mathbf{x}$ with $\mathbf{x}'$, the CNN will be fooled from the *true label* t to the *target (incorrect) label* t'. It was recently shown in (Xu et al., 2019b;a) that the adversary could introduce an evident *interpretability discrepancy* w.r.t. *both* the true and the target label in terms of $L(\mathbf{x}, t)$ vs. $L(\mathbf{x}', t)$, and $L(\mathbf{x}, t')$ vs. $L(\mathbf{x}', t')$. An illustrative example is provided in Figure 1. We see that an adversary *suppresses* the network interpretation w.r.t. the true label but *promotes* the interpretation w.r.t. the target label. We also observe that compared to IG, CAM and GradCAM++ better localize class-specific discriminative regions. The results imply both *pros and cons* of an interpreter L. On the *positive* side, the L allows the user to detect the misbehavior of a classifier (in terms of interpretability discrepancy) when facing adversarial examples. On the *negative* side, L might be vulnerable to a tiny change on the input (even for benign perturbation), which raises the question of the robustness in interpretability. In what follows, we explore the spectrum between adversarial robustness and interpretability from a unified attack-defense perspective.

3 Robustness in Classification or Interpretability? An Attack Perspective

In this section, we examine two types of threat models, *interpretability sneaking attack (ISA)* and *attack against interpretability (AAI)*, which craft perturbed inputs with intention to fool one of classifier and interpreter but to keep stealthiness from the other one. Since an adversarial example

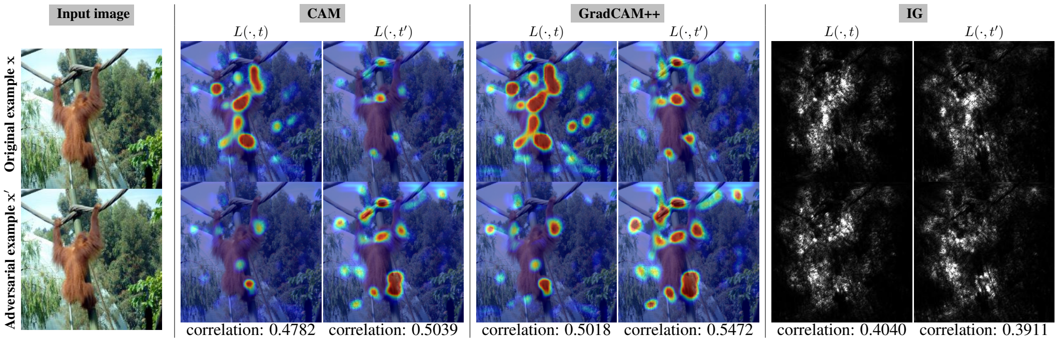

Figure 1: Interpretation (L) of benign ($\mathbf{x}$) and adversarial ($\mathbf{x}'$) image from restricted ImageNet (Engstrom et al., 2019) with respect to the true label t='monkey' and the target label t'='fish'. Here the adversarial example is generated by 10-step PGD attack with perturbation size 0.02 (Madry et al., 2018), and we consider three types of interpretation maps, CAM, GradCAM++ and IG. Given an interpretation method, the first column is $L(\mathbf{x}, t)$ versus $L(\mathbf{x}', t)$, the second column is $L(\mathbf{x}, t')$ versus $L(\mathbf{x}', t')$, and all maps under each category are normalized w.r.t. their largest value. At the bottom of each column, we quantify the resulting interpretability discrepancy by Kendall's Tau order rank correlation (Selvaraju et al., 2017) between every pair of $L(\mathbf{x}, i)$ and $L(\mathbf{x}', i)$ for $i = t$ or t'.

designed for misclassification gives rise to interpretability discrepancy (which could then be used as a detector for the adversarial input), the problem of ISA arises: One may wonder whether or not it is easy to generate adversarial examples that *mistake classification* but keep *interpretation intact*. One the other hand, it is suggested from interpretability discrepancy that an interpreter could be quite sensitive to input perturbations. Thus, the problem of AAI arises: One may wonder if perturbed inputs could induce *differing explanations* but *without altering predictions*.

3.1 Rethinking ISA from perspective of interpretability discrepancy

Previous work (Zhang et al., 2018; Subramanya et al., 2018) showed that it is *not difficult to hide* adversarial examples from network interpretation when the interpretability discrepancy is measured w.r.t. a *single* class label (either the true label t or the target label t'). However, we see from Figure 1 that the adversary (against classification) alters interpretability maps w.r.t. *both* t and t'. This motivates us to rethink whether the single-class interpretability discrepancy measure is proper, and whether ISA is truly easy to bypass an interpretability discrepancy check.

We consider the following generic form of interpretability discrepancy

$$\mathcal{D}\left(\mathbf{x}, \mathbf{x}'\right) = \frac{1}{|\mathcal{C}|} \sum_{i \in \mathcal{C}} \left\| L(\mathbf{x}, i) - L(\mathbf{x}', i) \right\|_p, \tag{3}$$

where recall that $\mathbf{x}$ and $\mathbf{x}'$ are natural and adversarial examples respectively, L represents an interpreter, e.g., CAM or IG, $\mathcal{C}$ denotes the set of class labels used in L, $|\mathcal{C}|$ is the cardinality of $\mathcal{C}$, and we consider $p \in \{1, 2\}$ in this paper. Clearly, a specification of (3) relies on the choice of $\mathcal{C}$ and p. We specify (3) with $\mathcal{C} = \{t, t'\}$ and $p = 1$, leading to *ℓ_1 2-class interpretability discrepancy measure,*

$$\mathcal{D}_{2,\ell_1}\left(\mathbf{x}, \mathbf{x}'\right) = \frac{1}{2} \left(\left\| L(\mathbf{x}, t) - L(\mathbf{x}', t) \right\|_1 + \left\| L(\mathbf{x}, t') - L(\mathbf{x}', t') \right\|_1 \right). \tag{4}$$

Rationale behind ℓ_1 2-class discrepancy measure. Compared to the previous work (Zhang et al., 2018; Subramanya et al., 2018) using a single class label, we choose $\mathcal{C} = \{t, t'\}$[1], motivated by the fact that an interpretability discrepancy occurs w.r.t. both t and t' (Figure 1). Moreover, although Euclidean distance (namely, ℓ_2 norm or its square) is arguably one of the most commonly-used discrepancy metrics (Zhang et al., 2018), we show in Proposition 1 that the proposed interpretability discrepancy measure $\mathcal{D}_{2,\ell_1}\left(\mathbf{x}, \mathbf{x}'\right)$ has a non-trivial lower bound for any successful adversarial attack. This provides an explanation on why it could be difficult to hide adversarial examples from network interpretability methods. Moreover, ℓ_1 is an upper bound of the ℓ_2 norm and promotes the sparsity of interpretability discrepancy, which enforces pixels of L to stay intact when facing input perturbations.

[1] In addition to the *2-class* case, our experiments will also cover the *all-class* case $\mathcal{C} = [C]$.

Proposition 1. *Given a classifier $f(\mathbf{x}) \in \mathbb{R}^C$ and its interpreter $L(\mathbf{x}, c)$ for $c \in [C]$, suppose that the interpreter satisfies the completeness axiom, namely, $\sum_i [L(\mathbf{x}, c)]_i = f_c(\mathbf{x})$. For a natural example $\mathbf{x}$ and an adversarial example $\mathbf{x}'$ with prediction t and t' respectively, $\mathcal{D}_{2,\ell_1}(\mathbf{x}, \mathbf{x}')$ in* (4) *has the lower bound*

$$\mathcal{D}_{2,\ell_1}\left(\mathbf{x}, \mathbf{x}'\right) \geq \frac{1}{2}\left(f_t(\mathbf{x}) - f_{t'}(\mathbf{x})\right). \tag{5}$$

Proof: See proof in Appendix A. □

Proposition 1 connects $\mathcal{D}_{2,\ell_1}(\mathbf{x}, \mathbf{x}')$ with the classification margin $f_t(\mathbf{x}) - f_{t'}(\mathbf{x})$. Thus, if a classifier has a large classification margin on the natural example $\mathbf{x}$, it will be difficult to find a successful adversarial attack with small interpretability discrepancy. In other words, *constraining the interpretability discrepancy prevents misclassification* since generating adversarial examples becomes infeasible under $\mathcal{D}_{2,\ell_1}(\mathbf{x}, \mathbf{x}') < \frac{1}{2}\left(f_t(\mathbf{x}) - f_{t'}(\mathbf{x})\right)$. Also, the completeness condition of L suggests specifying (4) with CAM (1) or IG (2). Here we focus on CAM due to its light computation.

Design of ISA. We pose the following optimization problem for design of ISA, which not only fools a classifier's decision but also minimizes the resulting interpretability discrepancy,

$$\begin{array}{ll} \underset{\boldsymbol{\delta}}{\text{minimize}} & \lambda \max\{\max_{j \neq t'} f_j(\mathbf{x} + \boldsymbol{\delta}) - f_{t'}(\mathbf{x} + \boldsymbol{\delta}), -\tau\} + \mathcal{D}_{2,\ell_1}(\mathbf{x}, \mathbf{x} + \boldsymbol{\delta}) \\ \text{subject to} & \|\boldsymbol{\delta}\|_\infty \leq \epsilon, \end{array} \tag{6}$$

where $\lambda > 0$ is a regularization parameter that strikes a balance between the success of an attack and its resulting interpretability discrepancy, $\tau \geq 0$ (e.g., 0.1 used in the paper) is a tolerance on the classification margin of a successful attack between the target label t' and the non-target top-1 prediction label $\arg\max_{j \neq t'} f_j(\mathbf{x} + \boldsymbol{\delta})$, $\mathcal{D}_{2,\ell_1}$ was defined by (4), and $\epsilon > 0$ is a (pixel-level) perturbation size. In (6), the first term of the objective corresponds to a C&W-type attack loss (Carlini & Wagner, 2017), which reaches $-\tau$ if the attack succeeds in misclassification. To find ISA of *minimum* interpretability discrepancy, we perform a *bisection* on λ until there exists no successful attack that can be found when λ further decreases. Although we focus on ℓ_∞ attack in (6), but a similar formulation applies to ℓ_1 and ℓ_2 attacks. Attacks are found using PGD, with subgradients taken at non-differentiable points. We consider only targeted attacks to better evaluate the effect on interpretability of target classes, although this approach can be extended to an untargeted setting (e.g., by using the target label-free interpretability discrepancy measure introduced in the next section).

Difficulty of generating ISA versus interpretability discrepancy measure. Through an illustrative example in Figure 2, we elaborate on how the choice of interpretability discrepancy measure plays a crucial role in hiding adversarial examples from network interpretation. We refer readers to Sec. 5 for more experimental results. We generate ISA under different specifications of (3) for different values of perturbation size ϵ. Compared to ℓ_1/ℓ_2 1-class (true class t), ℓ_2 2-class, and ℓ_1/ℓ_2 all-class, we see that the ℓ_1 2-class interpretability discrepancy (4) cannot be easily mitigated even as the attack power (in terms of ϵ) increases. This is verified by a) its high interpretability discrepancy score and b) its flat slope of discrepancy score against ϵ in Figure 2-(a)&(b). Figure 2-(c) further shows CAMs of adversarial examples w.r.t. the true label t and the target label t' generated by ℓ_1 1/2/all-class ISAs. As we can see, both 1-class measure and all-class measure could give a *false* sense of ease of hiding adversarial examples. For ℓ_1 1-class ISA, although the interpretability discrepancy w.r.t. t is minimized, the discrepancy w.r.t. t' remains large, supported by the observation that ℓ_1 1-class ISA even yields a smaller correlation between $L(\mathbf{x}', t')$ and $L(\mathbf{x}, t')$ than PGD attack. Similarly, although the averaged discrepancy over all classes is minimized for ℓ_1 all-class ISA, discrepancies w.r.t. specific labels such as t and t' do not necessarily reduce.

3.2 Attack against Interpretability (AAI)

Different from ISA, AAI produces input perturbations to maximize the interpretability discrepancy while keeping the classification decision intact. Thus, AAI provides a means to evaluate the adversarial robustness in interpretability. Since $t = \arg\max_i f_i(\mathbf{x}) = \arg\max_i f_i(\mathbf{x}') = t'$ in AAI, the 2-class interpretability discrepancy measure (4) reduces to its 1-class version. The problem of generating AAI is then cast as

$$\begin{array}{ll} \underset{\boldsymbol{\delta}}{\text{minimize}} & \lambda \max\{\max_{j \neq t} f_j(\mathbf{x} + \boldsymbol{\delta}) - f_t(\mathbf{x} + \boldsymbol{\delta}), 0\} - \mathcal{D}_1(\mathbf{x}, \mathbf{x} + \boldsymbol{\delta}) \\ \text{subject to} & \|\boldsymbol{\delta}\|_\infty \leq \epsilon, \end{array} \tag{7}$$

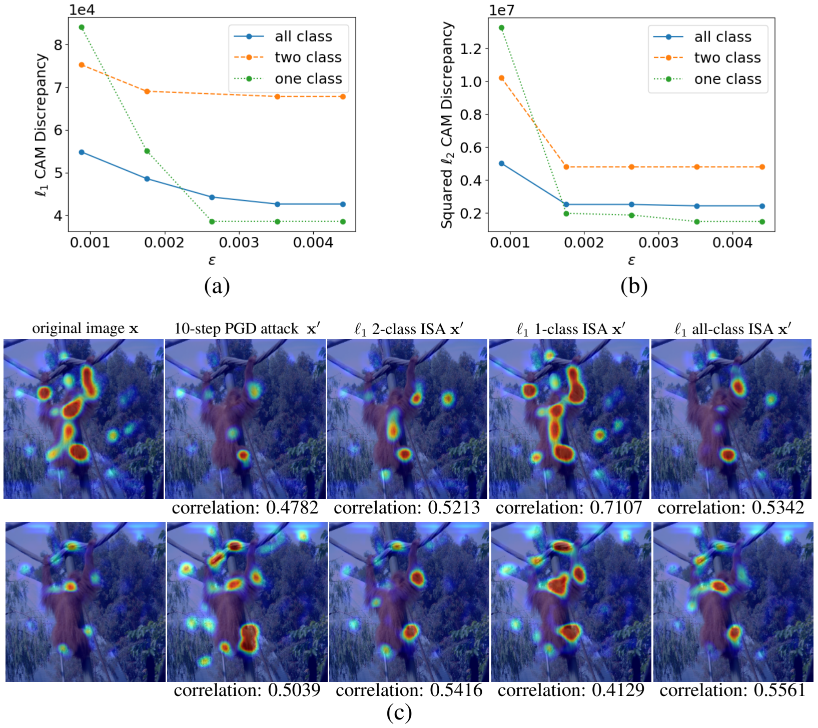

(a)

(b)

(c)

Figure 2: Seeing the effect of discrepancy measure on hiding adversarial examples from network interpretation. The same benign image in Figure 1 is considered. (a) ISA using CAM-based ℓ_1 1/2/all-class discrepancy measure versus perturbation size ϵ, (b) ISA using CAM-based squared ℓ_2 1/2/all-class discrepancy measure versus ϵ, (c) CAM interpretation of example in Figure 1 and its adversarial counterparts from PGD attack and different specifications of ISA. All interpretation maps are normalized w.r.t. their largest value. At the bottom of each interpretation map $L(\mathbf{x}', \cdot)$, we quantify the interpretability discrepancy by Kendall's Tau order rank correlation between every pair of $L(\mathbf{x}', i)$ and $L(\mathbf{x}', i)$ for $i \in \{t, t'\}$, where $\mathbf{x}'$ is obtained from PGD attack or each specification of ISA.

where the first term is a hinge loss to enforce $f_t(\mathbf{x} + \boldsymbol{\delta}) \geq \max_{j \neq t} f_j(\mathbf{x} + \boldsymbol{\delta})$, namely, $\arg\max_i f_i(\mathbf{x}') = t$ (unchanged prediction under input perturbations), and $\mathcal{D}_1$ denotes a 1-class interpretability discrepancy measure, e.g., $\mathcal{D}_{1,\ell_1}$ from (4), or the top-k pixel difference between interpretability maps (Ghorbani et al., 2019). Similar to (6), the regularization parameter λ in (7) strikes a balance between stealthiness in classification and variation in interpretability. Experiments in Sec. 5 will show that the state-of-the-art defense methods against adversarial examples do not necessarily preserve robustness in interpretability as ϵ increases, athough the prediction is not altered.

4 Interpretability-Aware Robust Training: Defense Perspective

We recall from Sec. 3.1 that adversarial examples that intend to fool a classifier could be difficult to evade the ℓ_1 2-class interpretability discrepancy. Thus, constraining the interpretability discrepancy helps to prevent misclassification. As an additional benefit, it also robustifies the classifier against AAI, where the adversary maximizes the interpretability discrepancy.

Target label-free interpretability discrepancy. Different from attack generation, the ℓ_1 2-class discrepancy measure (4) cannot directly be used by a defender since the target label t' specified by the adversary is *not* known *a priori*. To circumvent this issue, we propose to approximate the interpretability discrepancy w.r.t. the target label by weighting discrepancies from all non-true classes according to their importance in prediction. This modifies (4) to

$$\tilde{\mathcal{D}}\left(\mathbf{x}, \mathbf{x}'\right) = \frac{1}{2}\left\|L(\mathbf{x}, t) - L(\mathbf{x}', t)\right\|_1 + \frac{1}{2}\sum_{i \neq t} \frac{e^{f(\mathbf{x}')_i}}{\sum_i e^{f(\mathbf{x}')_i}} ||L(\mathbf{x}, i) - L(\mathbf{x}', i)||_1, \qquad (8)$$

where the softmax function $\frac{e^{f(\mathbf{x}')_i}}{\sum_i e^{f(\mathbf{x}')_i}}$ adjusts the importance of non-true labels according to their classification confidence. Clearly, when $\mathbf{x}'$ succeeds in misclassification, the top-1 predicted class of $\mathbf{x}'$ becomes the target label and the resulting interpretability discrepancy is most penalized.

Interpretability-aware robust training. We propose to train a classifier against the *worst-case* interpretability discrepancy (8), yielding the min-max optimization problem

$$\underset{\boldsymbol{\theta}}{\text{minimize}} \ \mathbb{E}_{(\mathbf{x},t)\sim\mathcal{D}_{\text{train}}} \left[f_{\text{train}}(\boldsymbol{\theta};\mathbf{x},t) + \gamma \underset{\mathbf{x}':\|\mathbf{x}'-\mathbf{x}\|_\infty \leq \epsilon}{\text{maximize}} \tilde{\mathcal{D}}\left(\mathbf{x},\mathbf{x}'\right) \right], \tag{9}$$

where $\boldsymbol{\theta}$ denotes the model parameters, $\mathcal{D}_{\text{train}}$ denotes the training dataset, f_{train} is the training loss (e.g., cross-entropy loss), $\gamma > 0$ is a regularization parameter, and for ease of notation we omit the parameters $\boldsymbol{\theta}$ and t in $\tilde{\mathcal{D}}\left(\mathbf{x},\mathbf{x}'\right)$.

In problem (9), the inner maximization is only used to evaluate the worst-case interpretability discrepancy. Thus, it is different from adversarial training (Madry et al., 2018), where the *training loss* is replaced with the *adversarial loss* $\text{maximize}_{\mathbf{x}':\|\mathbf{x}'-\mathbf{x}\|_\infty \leq \epsilon} f_{\text{train}}(\boldsymbol{\theta},\mathbf{x}';\mathbf{x},t)$. The formulation (9) allows us to examine whether or not robust interpretation is directly beneficial to robust classification. For completeness, we will also provide experiment results on a modified formulation of (9) with the use of the adversarial loss.

Difference to (Chen et al., 2019). The recent work (Chen et al., 2019) proposed improving adversarial robustness by leveraging robust IG attributions. However, different from (Chen et al., 2019), our approach is motivated by the importance of ℓ_1 2-class interpretability discrepancy measure. We will show in Sec. 5 that the incorporation of interpretability discrepancy w.r.t. target class labels, namely, the second term in (8), plays a key role in boosting classification and interpretation robustness. We will also show that our proposed method is sufficient to improve adversarial robustness even in the absence of adversarial loss, while the robust attribution regularization method (Chen et al., 2019) becomes ineffective when the attack becomes stronger. Last but not the least, beyond IG, our proposed theory and method apply to any network interpretation method with completeness axiom. The use of CAM avoids Riemman approximation used in IG and thus simplifies the implementation during robust training.

5 Experiments

In this section, we empirically show the effectiveness of our proposed methods in various attack and defense settings. For ISA, we examine how the interpretability discrepancy measure plays a role in hiding adversarial examples from network interpretation. For AAI, we evaluate its attack success rate under the natural and various robust models. For interpretability-aware robust training, we demonstrate its advantages in a) defending against PGD attacks with different steps and perturbation sizes (Madry et al., 2018; Athalye et al., 2018), b) defending against unforeseen adversarial attacks (Kang et al., 2019), c) rendering robustness in interpretability, and d) computation efficiency compared to the IG-based robust attribution regularization method (Chen et al., 2019).

Datasets, CNN models, and experiment setting. We evaluate networks trained on the MNIST, CIFAR-10 and a restricted ImageNet (R-ImageNet) dataset used in (Engstrom et al., 2019). We consider three models, *Small* (for MNIST and CIFAR), *Pool* (for MNIST) and *WResnet* (for CIFAR and R-ImageNet): 1) a small CNN architecture consisting of three convolutional layers of 16, 32 and 100 filters (Small), 2) a CNN architecture with two convolutional layers of 32 and 64 filters each followed by max-pooling which is adapted from (Madry et al., 2018) (Pool), and 3) a Wide Resnet from (Madry et al., 2018) (WResnet). Each network has a global average pooling layer followed by a fully connected layer at the end of the network. For R-ImageNet, we use only a normally trained network, used for evaluating ISA. During adversarial training of all baselines, 40 adversarial steps are used for MNIST and 10 steps for CIFAR. To ensure stability of all training methods, the size of perturbation is increased during training from 0 to a final value of 0.3 on MNIST and 8/255 on CIFAR.

In the following experiments, we consider 5 *baselines* from the literature: i) standard training (*Normal*), ii) adversarial training (*Adv*) (Madry et al., 2018), iii) *TRADES* (Zhang et al., 2019), iv)

IG-Norm that uses IG-based robust attribution regularization (Chen et al., 2019), v) *IG-Sum-Norm* (namely, IG-Norm with adversarial loss). Additionally, we consider 3 *variants* of our method: vi) the proposed interpretability-aware robust training method (9) (we call *Int*), vii) Int using ℓ_1 1-class discrepancy (*Int-1-class*), and viii) Int with adversarial loss (*Int-Adv*).

Dataset	Interpretation method	ℓ_1 norm			ℓ_2 norm		
		1-class	2-class	all-class	1-class	2-class	all-class
MNIST	CAM	3.0723/0.0810	3.2672/0.0223	2.5289/0.0414	0.3061/0.1505	0.5654/0.0321	0.4320/0.0459
	GradCAM++	3.1264/0.0814	3.1867/0.0221	2.5394/0.0366	0.3308/0.1447	0.5531/0.0289	0.4392/0.0456
	IG	6.3604/0.0330	6.7884/0.0233	4.3667/0.2314	0.4476/0.0082	0.5766/0.0064	0.2160/0.0337
	Repr	n/a	2.3668/0.0404	n/a	n/a	0.4129/0.0429	n/a
CIFAR-10	CAM	1.9523/0.1450	2.5020/0.0496	1.7898/0.0774	0.1313/0.2369	0.3613/0.0668	0.2746/0.0809
	GradCAM++	1.9355/0.1439	2.4788/0.0513	1.8020/0.0745	0.1375/0.2346	0.3577/0.0676	0.2758/0.0769
	IG	4.9499/0.0188	4.9794/0.0177	2.8541/0.1356	0.1230/0.0110	0.1309/0.0092	0.0878/0.0235
	Repr	n/a	1.7049/0.0785	n/a	n/a	0.1288/0.0056	n/a
R-ImageNet	CAM	49.286/0.1005	61.975/0.0331	49.877/0.0557	1.9373/0.1526	2.6036/0.0791	2.0935/0.0863
	GradCAM++	39.761/0.1028	50.303/0.0453	42.390/0.0552	1.9185/0.1609	2.5869/0.0891	2.1151/0.0896
	Repr	n/a	46.892/0.0657	n/a	n/a	2.0730/0.0781	n/a

Table 1: NDS and NSL (format given by NDS/NSL) of successful ISAs generated under different specifications of interpretability discrepancy measure (3) and datasets MNIST, CIFAR-10 and R-ImageNet. Here a discrepancy measure with large NDS and small NSL indicates a strong resistance to ISA.

Evaluating ISA. We evaluate the effect of interpretability discrepancy measure on ease of finding ISAs. Spurred by Figure 2, such an effect is quantified by calculating minimum discrepancy required in generating ISAs against different values of perturbation size ϵ in (6). We conduct experiments over 4 network interpretation methods: i) CAM, ii) GradCAM++, iii) IG, and iv) internal representation at the penultimate (pre-softmax) layer (denoted by *Repr*). In order to fairly compare among different interpretation methods, we compute a *normalized discrepancy score (NDS)* extended from (3): $\mathcal{D}_{\mathrm{norm}} = \frac{1}{|\mathcal{C}|} \sum_{i \in \mathcal{C}} \left\| \frac{\mathcal{L}(\mathbf{x}, i) - \mathcal{L}(\mathbf{x}', i)}{\max_j L(\mathbf{x}, i)_j - \min_j L(\mathbf{x}, i)_j} \right\|_p$. A smaller value of NDS implies the less difficulty for ISA to hide adversarial examples. A strong ISA is also expected to resist interpretability discrepancy even as the perturbation size ϵ increases; see Figure 2-(a)&(b). To quantify this, we compute an additional quantity called *normalized slope (NSL)* that measures the relative change of NDS for $\epsilon \in [\check{\epsilon}, \hat{\epsilon}]$: $\mathcal{S}_{\mathrm{norm}} = \frac{|\mathcal{D}_{\mathrm{norm}}^{(\hat{\epsilon})} - \mathcal{D}_{\mathrm{norm}}^{(\check{\epsilon})}| / \mathcal{D}_{\mathrm{norm}}^{(\check{\epsilon})}}{(\hat{\epsilon} - \check{\epsilon}) / \check{\epsilon}}$. The smaller NDS is, the less strong ISA is to evade network interpretation change. In our experiment, we choose $\check{\epsilon} = \epsilon^*$ and $\hat{\epsilon} = 1.6\, \epsilon^*$, where ϵ^* is the minimum perturbation size required for a successful PGD attack for each image $\mathbf{x}$. Here we perform binary search over ϵ to find its smallest value for misclassification. Reported NDS and NSL statistics are averaged over a test set.

In Table 1, we present NDS and NSL of ISAs generated under different realizations of interpretability discrepancy measure (3), each of which is given by a combination of interpretation method (CAM, GradCAM++, IG or Repr), ℓ_p norm ($p \in \{1, 2\}$) and number of interpreted classes. Note that Repr is independent of the number of classes, and thus we report NDS and NSL corresponding to Repr in the 2-class column of Table 1. Given an ℓ_p norm and an interpretation method, we consistently find that the use of 2-class measure achieves the largest NDS and smallest NSL at the same time. This implies that the 2-class discrepancy measure increases the difficulty of ISA to evade network interpretability check. Moreover, given a class number and an interpretation method, we see that NDS under ℓ_1 norm is greater than that under ℓ_2 norm, since the former is naturally an upper bound of the latter. Also, the use of ℓ_1 norm often yields a smaller value of NSL, implying that the ℓ_1-norm based discrepancy measure is more resistant to ISA. Furthermore, by fixing the combination of ℓ_1 norm and 2 classes, we observe that IG is the most resistant to ISA due to their relatively high NDS and low ISA, and Repr yields the worst performance. However, compared to CAM, the computation cost of IG increases dramatically as the input dimension, the model size, and the number of steps in Riemman approximation increase. We find that it becomes infeasible to generate ISA using IG for WResnet under R-ImageNet within 200 hours.

Evaluating AAI. We specify problem (7) under the top-k attack setting (Ghorbani et al., 2017), where the top-k intersection between the original and adversarial interpretability maps is minimized. The strength of AAI is then measured by the Kendall's Tau order rank correlation between the aforementioned two interpretability maps (Chen et al., 2019). The higher the correlation is, the more robust the model is against AAI. Reported rank correlations are averaged over a test set.

In Table 2, we present the performance of AAI under multiple perturbation sizes to attack models trained using different training methods. For the model Small under MNIST, we evaluate AAI over 5 baselines (Normal, Adv, TRADES, IG-Norm, IG-Sum-Norm) and 3 variants of our method (Int, Int-1-class and Int-Adv). For a larger model WResnet under CIFAR-10, the training methods using IG (IG-Norm and IG-Norm-Sum) are excluded due to their prohibitive computation cost. The insights learnt from Table 2 are summarized as below. First, the normally trained model (Normal) does not automatically give robustness guarantees in interpretability, particularly for AAI with $\epsilon \geq 0.2$. Second, the methods Adv, TRADES, IG-Sum-Norm and Int-Adv that uses adversarial loss offer certain robustness against AAI but the performance gets worse as the perturbation size ϵ increases. Third, in the absence of adversarial loss, the baseline IG-Norm becomes less robust as ϵ increases. By contrast, our proposed method Int is consistently more robust and its advantage becomes more evident as ϵ increases.

Method	$\epsilon = 0.05$	0.1	0.2	0.3
	MNIST, Small			
Normal	0.907	0.797	0.366	-0.085
Adv	**0.978**	**0.955**	**0.910**	**0.857**
TRADES	**0.978**	**0.955**	0.905	0.847
IG-Norm	0.958	0.894	0.662	0.278
IG-Norm-Sum	0.976	0.951	0.901	0.850
Int	**0.982**	**0.968**	**0.941**	**0.913**
Int-Adv	**0.980**	**0.965**	**0.936**	**0.912**
Int-1-class	0.874	0.818	0.754	0.692
	$\epsilon = 2/255$	4/255	6/255	8/255
	CIFAR, WResnet			
Normal	0.595	0.159	0.067	-0.069
Adv	**0.912**	**0.816**	**0.724**	0.629
TRADES	**0.918**	**0.832**	**0.747**	**0.652**
Int	0.859	0.763	0.746	**0.682**
Int-Adv	**0.885**	**0.803**	**0.751**	**0.696**

Table 2: Performance of AAI for different values of perturbation size ϵ in terms of Kendall's Tau order rank correlation between the original and adversarial interpretability maps. Best robustness results (corresponding to highest correlation values) are highlighted (**1st**, **2nd**, **3rd**) under each column of a dataset-model pair.

Evaluating interpretability-aware robust training. We previously showed in Table 2 that interpretability-aware robust training (Int, Int-Adv) often achieves more robust interpretability than state-of-the-art adversarial training methods particularly for large perturbation size. In what follows, we provide a thorough evaluation on how interpretability helps adversarial robustness against misclassification.

Robustness versus efficiency. In Figure 3, we present the training time (left y-axis) and the adversarial test accuracy (right y-axis) for different training methods (x-axis), which are ranked in a decreasing order of computation complexity. Here the adversarial test accuracy (ATA) is measured using 200-step (ℓ_∞-norm) perturbation size $\epsilon = 0.3$ on the Small MNIST model (Madry et al., 2018). As we can see, all AT-type methods (IG-Norm-Sum, Int-Adv, TRADES and Adv) offer robust classification with ATA around 80%. Among non-AT but interpretability promoted defensive schemes (IG-Norm, Int, Int-1-class), we find that only the proposed Int yields competitive ATA. We will show that IG-Norm becomes much less robust in classification when PGD attack becomes stronger (see results in Table 4). Moreover, the non-robustness of Int-1-class verifies the importance of 2-class interpretability discrepancy measure on rendering robust classification. Last but not the least, Adv, TRADES and Int-based methods have similar computational complexity, but IG-based methods make training time (per epoch) significantly higher, 3 times more than Int-Adv even under the Small MNIST model.

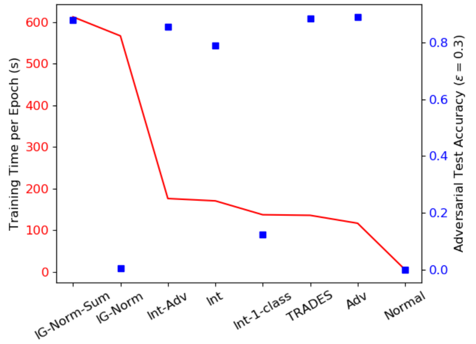

Figure 3: Computation time per epoch and adversarial test accuracy for a Small MNIST model trained with different methods.

*Int does **not** cause obfuscated gradients and importance of 2-class measure.* It was shown in (Athalye et al., 2018; Carlini, 2019) that some defense methods cause *obfuscated gradients*, which give a false sense of security. There exist two characteristic behaviors of obfuscated gradients: a) One-step attacks perform better than iterative attacks; b) Increasing distortion bound does not increase success. Motivated by that, we evaluate our interpretability-aware robust training methods under PGD attacks with a) different steps and b) different perturbation sizes. Table 3 reports ATA of interpretability-aware robust training relative to various baselines, where 200-step PGD attacks are conducted for $\epsilon \in \{0, 0.05, 0.1, 0.2, 0.3\}$. As we can see, ATA decreases as ϵ increases. Thus, our methods do not exhibit the behavior a) of obfuscated gradients. We also observe that across datasets and architectures, Int achieves comparable PGD accuracy on the largest evaluated ϵ to adversarial training (0.790 vs 0.890 on MNIST, 0.270 vs 0.170 on CIFAR). We highlight that such a robustness of classification is achieved by promoting robustness of interpretability alone (without using the adversarial loss). It is worth mentioning that IG-Norm fails to defend PGD attack with $\epsilon = 0.3$ for the Small MNIST model. We further note that Int-1-class performs much worse than Int, supporting the *importance of using 2-class* discrepancy measure (see Prop. 1). Besides robust classification, IG-Norm and Int-1-class are also not sufficient to render robustness in interpretation (Table 2). Next, Table 4 shows ATA of interpretability-aware robust training against k-step PGD attacks (examining behavior b) of obfuscated gradients), where $k \in \{1, 10, 100, 200\}$. As we can see, ATA decreases as k increases. This also suggests that the high robust accuracy from our methods is not a result of obfuscated gradients. Similar to Table 3, we see that compared to Int, IG-Norm and Int-1-class are insufficient to defend PGD attacks with $k \geq 100$.

Beyond ℓ_∞-norm PGD attacks. In Table 5, we present ATA of interpretability-aware robust training and various baselines for defending attacks (Gabor, Snow, JPEG ℓ_∞, JPEG ℓ_2, and JPEG ℓ_1) recently proposed in (Kang et al., 2019). These attacks are called ‘unforseen attacks’ since they are not met by PGD-based robust training and often induce larger perturbations than conventional PGD attacks. For robust training methods without resorting to adversarial loss, we find that Int significantly outperforms IG-Norm especially under Snow and JPEG ℓ_p attacks. Int also yields quite competitive robustness compared to AT-type methods, verifying that interpretability alone could help adversarial robustness.

Method	$\epsilon = 0$	0.05	0.1	0.2	0.3
	MNIST, Small				
Normal	**1.000**	0.530	0.045	0.000	0.000
Adv	**0.980**	**0.960**	**0.940**	**0.925**	**0.890**
TRADES	0.970	**0.970**	**0.955**	**0.930**	**0.885**
IG-Norm	**0.985**	**0.950**	0.895	0.410	0.005
IG-Norm-Sum	0.975	0.955	0.935	**0.910**	0.880
Int-1-class	0.975	0.635	0.330	0.140	0.125
Int	0.935	0.930	0.905	0.840	0.790
Int-Adv	0.950	0.945	0.905	0.880	**0.855**
	$\epsilon = 2/255$	4/255	6/255	8/255	
	CIFAR, WResnet				
Normal	**0.765**	0.250	0.070	0.060	0.060
Adv	**0.720**	**0.605**	**0.485**	**0.330**	**0.170**
TRADES	**0.765**	**0.610**	**0.460**	0.295	**0.170**
Int	**0.735**	**0.630**	**0.485**	**0.365**	**0.270**
Int-Adv	0.665	0.585	**0.510**	**0.385**	**0.320**
Int-1-class	0.685	0.505	0.360	0.190	0.065

Table 3: 200-step PGD accuracy for different values of perturbation size ϵ. Best ATA results are highlighted (**1st**, **2nd**, **3rd**) at each column. Note that ATA with $\epsilon = 0$ reduces to natural accuracy.

Method	Steps= 1	10	100	200
	MNIST, Small, $\epsilon = 0.3$			
Normal	**0.990**	0.070	0.000	0.000
Adv	**0.975**	**0.945**	**0.890**	**0.890**
TRADES	**0.970**	**0.955**	**0.885**	**0.885**
IG-Norm	**0.970**	0.905	0.005	0.005
IG-Norm-Sum	0.970	**0.940**	**0.880**	**0.880**
Int-1-class	0.950	0.365	0.125	0.125
Int	0.935	0.910	0.790	0.790
Int-Adv	0.950	0.905	0.855	0.855
	CIFAR, Wresnet, $\epsilon = 8/255$			
Normal	0.470	0.075	0.060	0.060
Adv	**0.590**	**0.205**	**0.185**	**0.185**
TRADES	**0.590**	0.180	0.165	0.165
Int	**0.620**	**0.310**	**0.275**	**0.275**
Int-Adv	**0.580**	**0.345**	**0.335**	**0.335**
Int-1-class	0.505	0.100	0.060	0.060

Table 4: Multi-step PGD accuracy. Best ATA results are highlighted (**1st**, **2nd**, **3rd**) at each column.

6 Conclusion

In this paper, we investigate the connection between network interpretability and adversarial robustness. We show theoretically and empirically that with the correct choice of discrepancy measure, it is difficult to hide adversarial examples from interpretation. We leverage this discrepancy measure to develop a interpretability-aware robust training method that displays 1) high classification robustness in a variety of settings and 2) high robustness of interpretation.

Method	Gabor	Snow	JPEG ℓ_∞	JPEG ℓ_2	JPEG ℓ_1
	CIFAR-10, Small				
Normal	0.125	0.000	0.000	0.030	0.000
Adv	**0.190**	**0.115**	**0.460**	**0.380**	**0.230**
TRADES	**0.220**	0.085	0.425	0.300	0.070
IG-Norm	0.155	0.015	0.000	0.000	0.000
IG-Norm-Sum	**0.185**	**0.110**	**0.480**	**0.375**	0.215
Int	0.160	0.105	**0.440**	**0.345**	**0.260**
Int-Adv	0.150	**0.120**	0.340	0.310	**0.235**

Table 5: ATA on different unforeseen attacks in (Kang et al., 2019). Best results in each column are highlighted (**1st**, **2nd**, **3rd**)

References

Anish Athalye, Logan Engstrom, Andrew Ilyas, and Kevin Kwok. Synthesizing robust adversarial examples. *arXiv preprint arXiv:1707.07397*, 2017.

Anish Athalye, Nicholas Carlini, and David Wagner. Obfuscated gradients give a false sense of security: Circumventing defenses to adversarial examples. *ICML*, arXiv preprint arXiv:1802.00420, 2018.

David Bau, Bolei Zhou, Aditya Khosla, Aude Oliva, and Antonio Torralba. Network dissection: Quantifying interpretability of deep visual representations. In *Proceedings of the IEEE Conference on Computer Vision and Pattern Recognition*, pp. 6541–6549, 2017.

Tom B Brown, Dandelion Mané, Aurko Roy, Martín Abadi, and Justin Gilmer. Adversarial patch. *arXiv preprint arXiv:1712.09665*, 2017.

Nicholas Carlini. Is ami (attacks meet interpretability) robust to adversarial examples? *arXiv preprint arXiv:1902.02322*, 2019.

Nicholas Carlini and David Wagner. Towards evaluating the robustness of neural networks. In *IEEE Symposium on Security and Privacy (SP)*, pp. 39–57. IEEE, 2017.

Aditya Chattopadhay, Anirban Sarkar, Prantik Howlader, and Vineeth N Balasubramanian. Grad-CAM++: Generalized gradient-based visual explanations for deep convolutional networks. In *2018 IEEE Winter Conference on Applications of Computer Vision (WACV)*, pp. 839–847. IEEE, 2018.

Jiefeng Chen, Xi Wu, Vaibhav Rastogi, Yingyu Liang, and Somesh Jha. Robust attribution regularization, 2019.

Pin-Yu Chen, Yash Sharma, Huan Zhang, Jinfeng Yi, and Cho-Jui Hsieh. Ead: elastic-net attacks to deep neural networks via adversarial examples. *AAAI*, 2018.

Ann-Kathrin Dombrowski, Maximilian Alber, Christopher J Anders, Marcel Ackermann, Klaus-Robert Müller, and Pan Kessel. Explanations can be manipulated and geometry is to blame. *arXiv preprint arXiv:1906.07983*, 2019.

Logan Engstrom, Andrew Ilyas, Shibani Santurkar, Dimitris Tsipras, Brandon Tran, and Aleksander Madry. Learning perceptually-aligned representations via adversarial robustness. *arXiv preprint arXiv:1906.00945*, 2019.

K. Eykholt, I. Evtimov, E. Fernandes, B. Li, A. Rahmati, C. Xiao, A. Prakash, T. Kohno, and D. Song. Robust physical-world attacks on deep learning visual classification. In *Proceedings of the IEEE Conference on Computer Vision and Pattern Recognition*, pp. 1625–1634, 2018.

Amirata Ghorbani, Abubakar Abid, and James Zou. Interpretation of neural networks is fragile. *arXiv preprint arXiv:1710.10547*, 2017.

Amirata Ghorbani, Abubakar Abid, and James Zou. Interpretation of neural networks is fragile. In *Proceedings of the AAAI Conference on Artificial Intelligence*, volume 33, pp. 3681–3688, 2019.

Ian Goodfellow, Jonathon Shlens, and Christian Szegedy. Explaining and harnessing adversarial examples. *ICLR*, arXiv preprint arXiv:1412.6572, 2015.

Daniel Kang, Yi Sun, Dan Hendrycks, Tom Brown, and Jacob Steinhardt. Testing robustness against unforeseen adversaries. *arXiv preprint arXiv:1908.08016*, 2019.

Aleksander Madry, Aleksandar Makelov, Ludwig Schmidt, Dimitris Tsipras, and Adrian Vladu. Towards deep learning models resistant to adversarial attacks. *ICLR*, arXiv preprint arXiv:1706.06083, 2018.

Seyed-Mohsen Moosavi-Dezfooli, Alhussein Fawzi, Jonathan Uesato, and Pascal Frossard. Robustness via curvature regularization, and vice versa. In *Proceedings of the IEEE Conference on Computer Vision and Pattern Recognition*, pp. 9078–9086, 2019.

Nicolas Papernot, Patrick McDaniel, Somesh Jha, Matt Fredrikson, Z Berkay Celik, and Ananthram Swami. The limitations of deep learning in adversarial settings. In *IEEE European Symposium on Security and Privacy (EuroS&P)*, pp. 372–387. IEEE, 2016a.

Nicolas Papernot, Patrick McDaniel, Xi Wu, Somesh Jha, and Ananthram Swami. Distillation as a defense to adversarial perturbations against deep neural networks. In *2016 IEEE Symposium on Security and Privacy (SP)*, pp. 582–597. IEEE, 2016b.

Vitali Petsiuk, Abir Das, and Kate Saenko. Rise: Randomized input sampling for explanation of black-box models. *arXiv preprint arXiv:1806.07421*, 2018.

Andrew Slavin Ross and Finale Doshi-Velez. Improving the adversarial robustness and interpretability of deep neural networks by regularizing their input gradients. In *Thirty-second AAAI conference on artificial intelligence*, 2018.

Ramprasaath R Selvaraju, Michael Cogswell, Abhishek Das, Ramakrishna Vedantam, Devi Parikh, and Dhruv Batra. Grad-CAM: Visual explanations from deep networks via gradient-based localization. In *Proceedings of the IEEE International Conference on Computer Vision*, pp. 618–626, 2017.

Karen Simonyan, Andrea Vedaldi, and Andrew Zisserman. Deep inside convolutional networks: Visualising image classification models and saliency maps. *arXiv preprint arXiv:1312.6034*, 2013.

Daniel Smilkov, Nikhil Thorat, Been Kim, Fernanda Viégas, and Martin Wattenberg. Smoothgrad: removing noise by adding noise. *arXiv preprint arXiv:1706.03825*, 2017.

Jost Tobias Springenberg, Alexey Dosovitskiy, Thomas Brox, and Martin Riedmiller. Striving for simplicity: The all convolutional net. *arXiv preprint arXiv:1412.6806*, 2014.

Dong Su, Huan Zhang, Hongge Chen, Jinfeng Yi, Pin-Yu Chen, and Yupeng Gao. Is robustness the cost of accuracy?–a comprehensive study on the robustness of 18 deep image classification models. *arXiv preprint arXiv:1808.01688*, 2018.

Akshayvarun Subramanya, Vipin Pillai, and Hamed Pirsiavash. Towards hiding adversarial examples from network interpretation. *arXiv preprint arXiv:1812.02843*, 2018.

Mukund Sundararajan, Ankur Taly, and Qiqi Yan. Axiomatic attribution for deep networks. In *Proceedings of the 34th International Conference on Machine Learning-Volume 70*, pp. 3319–3328. JMLR. org, 2017.

Christian Szegedy, Wojciech Zaremba, Ilya Sutskever, Joan Bruna, Dumitru Erhan, Ian Goodfellow, and Rob Fergus. Intriguing properties of neural networks. *ICLR*, arXiv preprint arXiv:1312.6199, 2014.

Kaidi Xu, Sijia Liu, Gaoyuan Zhang, Mengshu Sun, Pu Zhao, Quanfu Fan, Chuang Gan, and Xue Lin. Interpreting adversarial examples by activation promotion and suppression. *arXiv preprint arXiv:1904.02057*, 2019a.

Kaidi Xu, Sijia Liu, Pu Zhao, Pin-Yu Chen, Huan Zhang, Quanfu Fan, Deniz Erdogmus, Yanzhi Wang, and Xue Lin. Structured adversarial attack: Towards general implementation and better interpretability. In *International Conference on Learning Representations*, 2019b.

Chih-Kuan Yeh, Cheng-Yu Hsieh, Arun Sai Suggala, David Inouye, and Pradeep Ravikumar. On the (in)fidelity and sensitivity for explanations, 2019.

Matthew D Zeiler and Rob Fergus. Visualizing and understanding convolutional networks. In *European conference on computer vision*, pp. 818–833. Springer, 2014.

Hongyang Zhang, Yaodong Yu, Jiantao Jiao, Eric P Xing, Laurent El Ghaoui, and Michael I Jordan. Theoretically principled trade-off between robustness and accuracy. *arXiv preprint arXiv:1901.08573*, 2019.

Xinyang Zhang, Ningfei Wang, Shouling Ji, Hua Shen, and Ting Wang. Interpretable deep learning under fire. *CoRR*, abs/1812.00891, 2018. URL `http://arxiv.org/abs/1812.00891`.

B. Zhou, A. Khosla, A. Lapedriza, A. Oliva, and A. Torralba. Learning deep features for discriminative localization. In *Proceedings of the IEEE Conference on Computer Vision and Pattern Recognition*, pp. 2921–2929, 2016.

APPENDIX

A PROOF OF PROPOSITION 1

For $\forall c \in [C]$, by the completeness axiom we have $f_c(\mathbf{x}) = \sum_i [L(\mathbf{x}, c)]_i$. Using this fact, we obtain that

$$\begin{aligned} f_{t'}(\mathbf{x}') - f_{t'}(\mathbf{x}) &= \sum_i ([L(\mathbf{x}', t')]_i - [L(\mathbf{x}, t')]_i) \\ &\leq \sum_i |[L(\mathbf{x}', t')]_i - [L(\mathbf{x}, t')]_i| = \|L(\mathbf{x}', t') - L(\mathbf{x}, t')\|_1. \end{aligned} \tag{10}$$

Similarly, we have

$$f_t(\mathbf{x}) - f_t(\mathbf{x}') \leq \|L(\mathbf{x}, t) - L(\mathbf{x}', t)\|_1. \tag{11}$$

Adding (10) and (11) rearranging yields

$$[f_{t'}(\mathbf{x}') - f_t(\mathbf{x}')] + [f_t(\mathbf{x}) - f_{t'}(\mathbf{x})] \leq \|L(\mathbf{x}', t') - L(\mathbf{x}, t')\|_1 + \|L(\mathbf{x}, t) - L(\mathbf{x}', t)\|_1. \tag{12}$$

Since $f_{t'}(\mathbf{x}') - -f_t(\mathbf{x}') \geq 0$, we then have $\|L(\mathbf{x}', t') - L(\mathbf{x}, t')\|_1 + \|L(\mathbf{x}, t) - L(\mathbf{x}', t)\|_1 \geq f_t(\mathbf{x}) - f_{t'}(\mathbf{x})$, which is equivalent to (5).

B Additional Tables

Method	$\epsilon = 0$	0.05	0.1	0.2	0.3
MNIST, Pool					
Normal	0.990	0.435	0.070	0.000	0.000
Adv	0.930	0.885	0.835	0.695	0.535
TRADES	0.955	0.910	0.870	0.720	0.455
IG-Norm	0.980	0.940	0.660	0.050	0.000
IG-Norm-Sum	0.920	0.885	0.840	0.700	0.540
Int	0.950	0.930	0.875	0.680	0.390
Int-Adv	0.870	0.840	0.810	0.755	0.690
Int-1-class	0.975	0.885	0.720	0.200	0.130
	$\epsilon = 0$	2/255	4/255	6/255	8/255
CIFAR-10, Small					
Normal	0.650	0.015	0.000	0.000	0.000
Adv	0.505	0.470	0.380	0.330	0.285
TRADES	0.630	0.465	0.355	0.235	0.140
IG-Norm	0.525	0.435	0.360	0.295	0.230
IG-Norm-Sum	0.390	0.365	0.325	0.310	0.285
Int	0.530	0.450	0.345	0.290	0.215
Int-Adv	0.675	0.145	0.005	0.000	0.000
Int-1-class	0.515	0.450	0.380	0.315	0.265

Table A1: 200 steps PGD accuracy, additional results.

Method	$\epsilon = 0$	0.05	0.1	0.2	0.3
MNIST, Pool					
Normal	0.990	0.435	0.070	0.000	0.000
Adv	0.930	0.885	0.835	0.695	0.535
TRADES	0.955	0.910	0.870	0.720	0.460
IG-Norm	0.980	0.945	0.660	0.060	0.000
IG-Norm-Sum	0.920	0.885	0.840	0.700	0.540
Int	0.950	0.930	0.875	0.680	0.385
Int-Adv	0.870	0.840	0.810	0.755	0.700
Int-1-class	0.975	0.885	0.720	0.200	0.130
	$\epsilon = 0$	2/255	4/255	6/255	8/255
CIFAR-10, Small					
Normal	0.650	0.015	0.000	0.000	0.000
Adv	0.505	0.470	0.380	0.330	0.285
TRADES	0.630	0.465	0.355	0.235	0.140
IG-Norm	0.525	0.435	0.360	0.295	0.230
IG-Norm-Sum	0.390	0.365	0.325	0.310	0.285
Int	0.530	0.450	0.345	0.290	0.215
Int-Adv	0.675	0.145	0.005	0.000	0.000
Int-1-class	0.515	0.450	0.380	0.315	0.265

Table A2: 100 step PGD accuracy, additional results.

Method	$\epsilon = 0$	0.05	0.1	0.2	0.3
MNIST, Pool					
Normal	0.990	0.470	0.135	0.135	0.135
Adv	0.930	0.885	0.845	0.845	0.845
TRADES	0.955	0.910	0.870	0.870	0.870
IG-Norm	0.980	0.945	0.705	0.705	0.705
IG-Norm-Sum	0.920	0.885	0.850	0.850	0.850
Int	0.950	0.930	0.885	0.885	0.885
Int-Adv	0.870	0.840	0.810	0.810	0.810
Int-1-class	0.975	0.885	0.750	0.750	0.750
	$\epsilon = 0$	2/255	4/255	6/255	8/255
CIFAR-10, Small					
Normal	0.650	0.015	0.000	0.000	0.000
Adv	0.505	0.470	0.380	0.325	0.280
TRADES	0.630	0.465	0.360	0.240	0.145
IG-Norm	0.675	0.145	0.005	0.000	0.000
IG-Norm-Sum	0.515	0.450	0.380	0.315	0.265
Int	0.525	0.435	0.360	0.295	0.235
Int-Adv	0.390	0.365	0.325	0.310	0.285
Int-1-class	0.530	0.450	0.345	0.290	0.220

Table A3: 10 step PGD accuracy, additional results.

Method	$\epsilon = 0.05$	0.1	0.2	0.3
MNIST, Pool				
Normal	0.934	0.876	0.719	0.482
Adv	0.976	0.951	0.896	0.824
TRADES	0.976	0.952	0.891	0.815
IG-Norm	0.942	0.872	0.648	0.341
IG-Norm-Sum	0.976	0.951	0.895	0.824
Int	0.964	0.928	0.852	0.771
Int-Adv	0.977	0.957	0.921	0.891
Int-1-class	0.930	0.871	0.779	0.704
	$\epsilon = 2/255$	4/255	6/255	8/255
CIFAR-10, Small				
Normal	0.694	0.350	0.116	-0.031
Adv	0.958	0.907	0.849	0.783
TRADES	0.940	0.867	0.781	0.689
IG-Norm	0.810	0.552	0.308	0.131
IG-Norm-Sum	0.958	0.907	0.847	0.779
Int	0.965	0.926	0.883	0.840
Int-Adv	0.979	0.956	0.931	0.904
Int-1-class	0.961	0.918	0.871	0.820

Table A4: Kendall rank correlation coefficients of top-k CAM attacks against interpretability found using 200 steps of PGD, additional results.

Method	$\epsilon = 0.05$	0.1	0.2	0.3
	MNIST, Pool			
Normal	0.957	0.912	0.811	0.594
Adv	0.978	0.955	0.903	0.839
TRADES	0.978	0.955	0.900	0.822
IG-Norm	0.979	0.955	0.879	0.771
IG-Norm-Sum	0.979	0.956	0.905	0.843
Int	0.949	0.893	0.759	0.588
Int-Adv	0.983	0.967	0.938	0.909
Int-1-class	0.934	0.858	0.747	0.717
	$\epsilon = 2/255$	4/255	6/255	8/255
	CIFAR-10, Small			
Normal	0.691	0.335	0.118	-0.031
Adv	0.958	0.908	0.850	0.781
TRADES	0.939	0.866	0.779	0.690
IG-Norm	0.805	0.546	0.303	0.117
IG-Norm-Sum	0.957	0.906	0.844	0.773
Int	0.964	0.925	0.881	0.831
Int-Adv	0.975	0.949	0.919	0.886
Int-1-class	0.959	0.914	0.861	0.803

Table A5: Kendall rank correlation coefficients of top-k GradCAM++ attacks against interpretability found using 200 steps of PGD, additional results.